Eur. Phys. J. E (2011) **34**: 24
DOI 10.1140/epje/i2011-11024-9

THE EUROPEAN PHYSICAL JOURNAL E

Regular Article

Delayed coalescence of droplets with miscible liquids: Lubrication and phase field theories*

R. Borcia[1,a], S. Menzel[1], M. Bestehorn[1], S. Karpitschka[2], and H. Riegler[2]

[1] Lehrstuhl Statistische Physik/Nichtlineare Dynamik Brandenburgische Technische Universität, D-03046 Cottbus, Germany
[2] Max-Planck-Institut für Kolloid und Grenzflächenforschung, Am Mühlenberg, D-14476 Potsdam, Germany

Received 12 July 2010
Published online: 7 March 2011 –

Abstract. Mixing of droplets with a body of different liquids shows an interesting behavior for small contact angles at solid substrate. The droplets interact with each other, a liquid exchange appears between the approaching drops owing to surface tension gradients at the droplets interface. But the drops remain separated for some seconds (up to minutes), until the merging into a single drop occurs (Langmuir **24**, 6395 (2008)). We investigate this phenomenon using lubrication approximation and phase field approach. For both methods, 2D quantitative computer simulations for delayed fusion of perfectly miscible thin liquid films/droplets with low contact angles are reported.

1 Introduction

Processes involving controlled motion and coalescence of fluid droplets have been intensively investigated in the last years owing to their scientific interest and practical significance (see refs. [1–5], and references therein). The scientific interest is strongly stimulated by the fact that these phenomena provide simple and quite beautiful examples of pattern formation. The practical importance is connected with a large number of industrial applications such as emulsion stability, ink-jet printing or coating applications.

The delayed coalescence of various combinations of miscible liquids was investigated first 1938 by D.H. Bangham and Z. Saweris [6]. They observed a strange behavior of the spreading drops, depending much on the properties of the adsorbed film at the solid/gas interface and on the surface tension. Recent qualitative experiments were performed by H. Riegler and P. Lazar [4]. They observed that sessile droplets of completely miscible liquids do not instantaneously coalesce after lateral contact if their contact angles are sufficiently small. A microscopically thin liquid bridge connects the droplets. Due to the surface tension gradients between the mixing droplets, a liquid exchange occurs through the bridging film (Marangoni effect). Under certain conditions, drops even chase each other across the substrate. Sometimes the drops are strongly pushed away from each other, and the interaction via bridging film is interrupted. In this case the drops remain separated, but mostly, after some seconds (up to minutes) the liquid from one droplet is completely driven by Marangoni forces into the second liquid droplet and the drops merge into a single one.

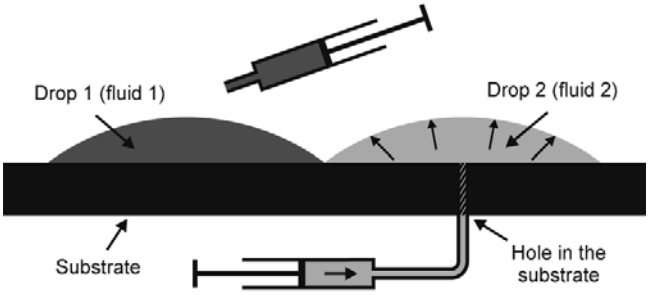

Fig. 1. Experimental setup for studying the coalescence of sessile drops.

Figure 1 shows an experimental setup designed for the study of the coalescence of two sessile droplets on a planar substrate [3]. The experiments were done in air (with air humidity below 5%). At first drop 1 (fluid 1) is deposited onto the substrate from the top with a syringe. Thus, its location, volume and state (receding or advancing contact angle) can be adjusted. Then, drop 2 with fluid 2 is created in the vicinity of drop 1. The position of drop 2 is fixed, but its volume can continuously be adjusted by pumping fluid 2 through a hole in the substrate. Upon increasing the volume of drop 2 its contact line will eventually come close enough to the contact line of drop 1 to initiate the

* Supplementary material in the form of two .avi files available from the Journal web page at
http://dx.doi.org/10.1140/epje/i2011-11024-9

[a] e-mail: borcia@physik.tu-cottbus.de

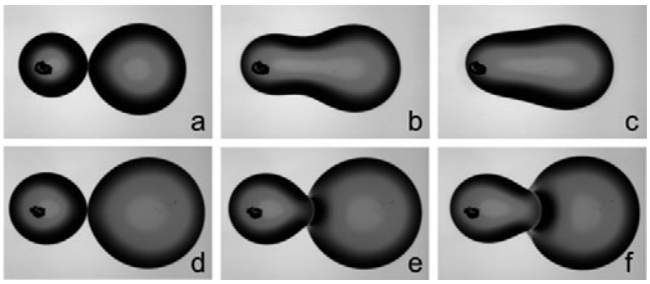

Fig. 2. Top views of the coalescence of sessile drops from different 1,2-propanediol/1,3-propanediol/water mixtures. Images (a)-(c): fast coalescence (50% 1,2-propanediol/50% water for both drops). Images (d)-(f): delayed coalescence (left drop as before, right drop now 25% 1,2-propanediol/25% 1,3-propanediol/50% water). Images (b) and (c) were taken, respectively, 0.41 s and 0.82 s after image (a); same applies to images (e) and (f) with respect to image (d).

coalescence process. This process can then be observed by optical imaging from the top and from the side.

Figure 2 shows drop coalescence experiments performed with the setup of fig. 1 with ternary mixtures of 1,2-propanediol, 1,3-propanediol and water (propanediols from Carl Roth, purity 99.5%). The water mass fraction was set to 50% for all drops, resulting in a viscosity of $5 \cdot 10^{-6}\,\mathrm{m}^2/\mathrm{s}$. The upper sequence (images (a), (b) and (c)) presents a fast droplet coalescence for identical liquids (pure 1,2-propanediol/water mixture). The image sequence (d), (e), and (f) presents a delayed coalescence (fluid 1: 50% propanediol/water; fluid 2: 25% 1,2-propanediol, 25% 1,3-propanediol/water). The frames were taken from two movies, which are available as additional supporting material. The videos were recorded at a frame rate of $61.5\,\mathrm{s}^{-1}$ and are set to playback at 30 frames/s, *i.e.* slowed down by a factor of ≈ 2. The substrate is silica[1]. The contact angle of all drops (frames (a) through (f)) is approximately the same around 10°. In fig. 2, the important difference between the sequences (a-c) and (d-f), respectively, is the surface tension. In the sequence (a) through (c) it is 0.045 N/m for both fluids. In the sequence (d) through (f) it is 0.045 N/m (fluid 1) *vs.* 0.05 N/m (fluid 2).

The gradient in surface tension is a decisive factor in the drop coalescence. The images displayed in figs. 2 and 3 and, specially, the video sequences supplied as additional material show that, the fast and the delayed coalescence can be clearly distinguished simply by varying the surface tension difference between the two droplets. The substantial difference between the coalescence modes can nicely be observed if one looks at the center-to-center profiles of the droplets during the coalescence process. These profiles could be resolved by using simple ray optics to evaluate simultaneously top and side view images (see fig. 3). Panel (a) shows the profiles from fig. 2(a-c) (fast coalescence), panel (b) those from fig. 2(d-f) (delayed coalescence).

[1] Si(100), p/Bor, 30 Ohm cm, available from SILCHEM, Freiberg, Germany, with natural oxide layer.

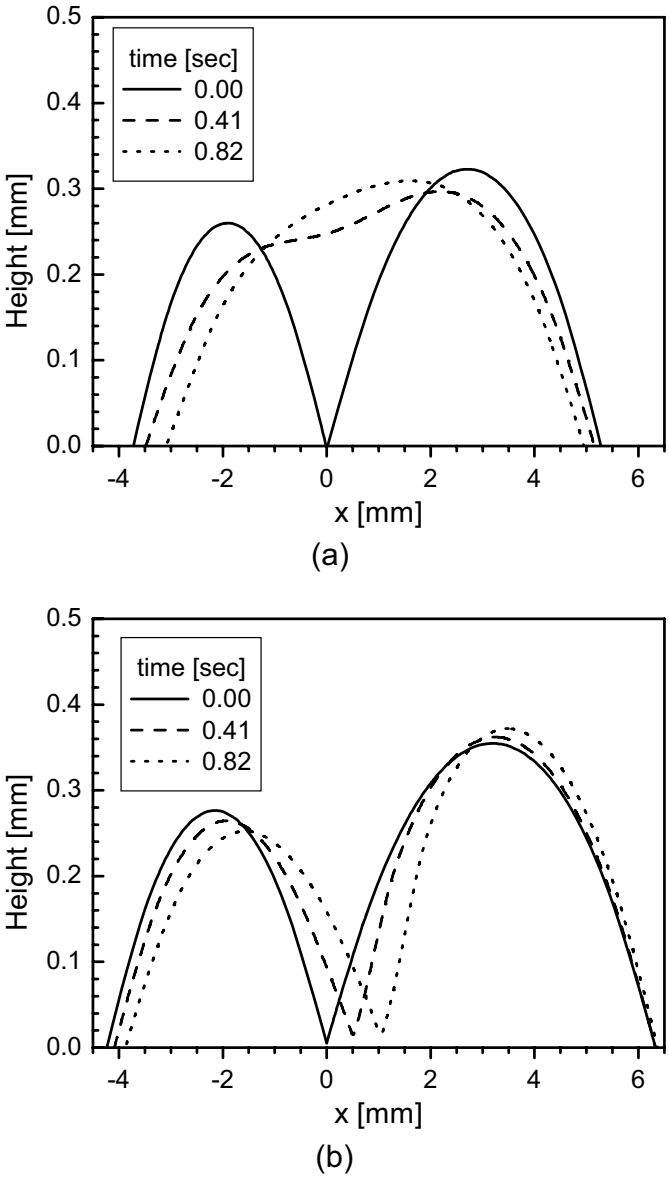

Fig. 3. Center-to-center profiles of the coalescence of sessile drops from the top imaging of fig. 2: (a) fast coalescence (50% 1,2-propanediol/50% water for both drops); (b) delayed coalescence (left drop: 50% 1,2-propane-diol/50% water: right drop: 25% 1,2-propanediol/25% 1,3-propanediol/50% water).

For the fast coalescence —illustrated in figs. 2(a-c)— the surface in the contact region between the two droplets levels out quickly, within 1 s (see fig. 3a). The connecting neck between the two drops fills up continuously, until the minimum of the liquid film between the interacting drops disappears. In the case of delayed coalescence —displayed in figs. 2(d-f)— the connecting film remains shallow, keeping the main droplet volumes separated for longer time (see fig. 3b). Even after 0.8 s the bridging film is low ($\leq 20\,\mu$m). The neck travels with a constant velocity of $v_{\mathrm{bridge}} = 1.33 \cdot 10^{-3}\,\mathrm{m/s}$ towards the drop with higher surface tension.

A recent study demonstrates that, for contact angles between 10° and 20°, a difference in surface tension be-

tween 3 and 5 mN/m leads to a rather sharp transition between the coalescence modes [7]. Viscosity seems to play a minor role, mostly determining the timescale of the coalescence process. In some experiments, small gas bubbles or dust particles were visible inside the drops, and due to their motion, a fast flow toward the droplet with the higher surface tension could be observed. This clearly proves that the Marangoni flow has an important role in different behaviors of droplets coalescence. A detailed experimental study on the dependence of the coalescence behavior with respect to liquid parameters can be found in [7].

The goal of this paper is to propose theoretical tools able to study the delayed coalescence of droplets with different perfectly miscible liquids. Two approaches are used in this paper: a lubrication approximation and a phase field model. Both models are compared to the droplet shape evolution in the experiments.

The lubrication approximation or long-wave-theory approach is based on the asymptotic reduction of the governing equations and boundary conditions to a simplified system which consists of a single partial differential equation formulated in terms of the local thickness of the film. In thin-film dynamics, the Reynolds numbers are small and one may usually neglect inertial forces compared to other forces like gravity or surface tension. Then velocity is enslaved by film thickness and one may derive the standard thin-film equation (see ref. [8], and references therein). So, the lubrication approximation reduces fully 3D problems to 2D descriptions (in two horizontal dimensions). This fact drastically reduces the computation time, making this approach very attractive for numerical simulations of thin liquid films. The long-wave theory showed considerable success in the past for investigating phase separation and drops/holes formation in binary liquid mixtures [9], Marangoni convection in one-layer and two-layers systems [10–12], pattern formation in ultrathin liquid layers [13], chemically driven drops on heterogeneous substrate [14,15] and, more recently, moving contact lines for small contact angles [16], and controlled pattern formation [17].

Another way to investigate numerically delayed droplets coalescence applies the phase field formalism. Consistent thermodynamical models are derived which treat multi-phase problems continuously. In the phase field method, to the usual set of variables an additional order parameter is introduced which takes different values for the coexisting phases. This variable is governed by a partial differential equation over the entire domain and is coupled to velocity, temperature, concentration fields, etc. The interface between two fluids is diffuse and is endowed with physical properties such as surface tension and captured implicitly by gradient terms of the phase field (see ref. [18], and references therein). So, the interface is not explicitly tracked in the phase field formalism. From this reason phase field models are flexible and very attractive to describe spatially and temporally varying interfaces with complicated geometries. This approach showed considerable success in the past to model solidification phenomena [19–21], dendritic growths [22,23], dynamic fractures [24], and, in hydrodynamics, for studying phase separation in binary liquids [18], spinoidal decomposition [25], Marangoni convection in two-phase systems [26–30], static contact angles, dynamic wetting [31–33], and controlled pattern formation in thin liquid layers [34].

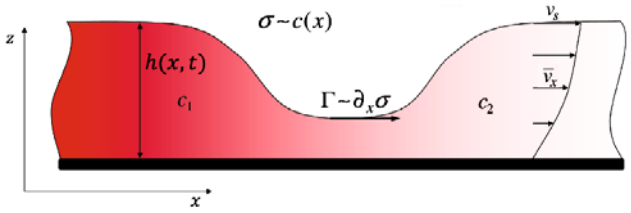

Fig. 4. (Color online) Sketch of the system. Two liquid films consisting of different perfectly miscible liquids are coming into contact through an ultrathin bridging film. The location of the upper deflecting interface $h(x,t)$ is a function of x and t only.

The paper is organized as follows: sect. 2 deals with the lubrication approximation. Governing equations are derived and numerical simulations in two-dimensions are performed for two thin liquid films with a body of different materials coming into contact through a gap. The phase field model equations together with corresponding 2D computer simulations for two approaching droplets with low contact angles are presented in sect. 3. We gather the conclusions in sect. 4.

2 Lubrication theory

2.1 Governing equations

We assume two liquid films consisting of two perfectly miscible liquids with the same density, the same viscosity, but with different surface tensions at the upper surface, situated at the height $z = h(x,t)$. The two thin liquid layers are connected through a bridging film, as sketched in fig. 4. Initially, the system is at rest on a rigid plate placed at $z = 0$.

One starts from the two-dimensional incompressible Navier-Stokes equations

$$\rho\left(\frac{\partial v_x}{\partial t} + v_x\frac{\partial v_x}{\partial x} + v_z\frac{\partial v_x}{\partial z}\right) = -\frac{\partial p}{\partial x} + \eta\left(\frac{\partial^2 v_x}{\partial x^2} + \frac{\partial^2 v_x}{\partial z^2}\right), \quad (1)$$

$$\rho\left(\frac{\partial v_z}{\partial t} + v_x\frac{\partial v_z}{\partial x} + v_z\frac{\partial v_z}{\partial z}\right) = -\frac{\partial p}{\partial z} + \eta\left(\frac{\partial^2 v_z}{\partial x^2} + \frac{\partial^2 v_z}{\partial z^2}\right) \quad (2)$$

and the continuity equation

$$\frac{\partial v_x}{\partial x} + \frac{\partial v_z}{\partial z} = 0, \quad (3)$$

with the following boundary conditions:

$$v_x|_{z=0} = 0, \qquad v_z|_{z=0} = 0, \quad (4)$$

the no-slip (and also no-penetration) condition at the lower boundary,

$$\frac{\partial h}{\partial t} = v_z|_{z=h} - v_x|_{z=h}\frac{\partial h}{\partial x}\,, \tag{5}$$

the kinematic boundary condition at the free surface, and

$$\eta\left(\frac{\partial v_x}{\partial z} + \frac{\partial v_z}{\partial x}\right)\bigg|_{z=h} = \frac{\partial \sigma}{\partial x}\,, \tag{6}$$

the balance of the tangential shear stresses at the upper boundary. In eqs. (1)–(2), p denotes the pressure and includes the Laplace pressure, $-\sigma\partial^2 h/\partial x^2$, σ is the surface tension coefficient, η is the dynamic viscosity.

We consider the long-wave approximation: $\delta = d/l \ll 1$, where d represents the mean depth of the film, and l is a typical lateral length. We scale the problem as follows:

$$t = t'\frac{l^2}{\nu}; \quad x = x'l; \quad z = z'd; \quad v_x = v_x'\frac{\nu}{l}; \quad v_z = v_z'\frac{\delta\nu}{l};$$
$$P = P'\frac{\rho\nu^2}{d^2}; \qquad \sigma = \sigma'\frac{\rho\nu^2}{d}\,,$$

with $\nu = \frac{\eta}{\rho}$ the kinematic viscosity.

After scaling eqs. (1)–(6) one gets (omitting the primes)

$$\delta^2\left(\frac{\partial v_x}{\partial t} + v_x\frac{\partial v_x}{\partial x} + v_z\frac{\partial v_x}{\partial z}\right) = -\frac{\partial p}{\partial x} + \left(\delta^2\frac{\partial^2}{\partial x^2} + \frac{\partial^2}{\partial z^2}\right)v_x, \tag{7}$$

$$\delta^4\left(\frac{\partial v_z}{\partial t} + v_x\frac{\partial v_z}{\partial x} + v_z\frac{\partial v_z}{\partial z}\right) = -\frac{\partial p}{\partial z} + \delta^2\left(\delta^2\frac{\partial^2}{\partial x^2} + \frac{\partial^2}{\partial z^2}\right)v_z, \tag{8}$$

$$\frac{\partial v_x}{\partial x} + \frac{\partial v_z}{\partial z} = 0, \tag{9}$$

$$v_x|_{z=0} = 0, \qquad v_z|_{z=0} = 0, \tag{10}$$

$$\frac{\partial h}{\partial t} = v_z|_{z=h} - v_x|_{z=h}\frac{\partial h}{\partial x}\,, \tag{11}$$

$$\eta\left(\frac{\partial v_x}{\partial z} + \delta^2\frac{\partial v_z}{\partial x}\right)\bigg|_{z=h} = \frac{\partial \sigma}{\partial x}\,. \tag{12}$$

In order δ^0, the above equations reduce to

$$-\frac{\partial p}{\partial x} + \frac{\partial^2 v_x}{\partial z^2} = 0, \tag{13}$$

$$\frac{\partial p}{\partial z} = 0, \tag{14}$$

$$\frac{\partial v_x}{\partial x} + \frac{\partial v_z}{\partial z} = 0, \tag{15}$$

$$v_x|_{z=0} = 0, \qquad v_z|_{z=0} = 0, \tag{16}$$

$$\frac{\partial h}{\partial t} = v_z|_{z=h} - v_x|_{z=h}\frac{\partial h}{\partial x}\,, \tag{17}$$

$$\frac{\partial v_x}{\partial z}\bigg|_{z=h} = \Gamma', \tag{18}$$

with $\Gamma' = \frac{1}{\eta}\frac{\partial \sigma}{\partial x}$.

From eq. (14) one can deduce that the pressure p depends only on the x coordinate. Equation (13) leads in this case to a quadratic velocity profile for $v_x = v_x(z)$

$$v_x(x,z,t) = a_1(x,t)z^2 + a_2(x,t)z + a_3(x,t).$$

Making use of the boundary conditions (16)–(18), one arrives at

$$v_x(x,z,t) = \left(\frac{\Gamma'}{h} - \frac{v_S}{h^2}\right)z^2 + \left(\frac{2v_S}{h} - \Gamma'\right)z, \tag{19}$$

where $v_S(x,t)$ is the velocity in x direction at the free surface.

We integrate the continuity equation (15) in the z-direction from 0 to $h(x,t)$ and use integration by parts, the boundary conditions (16) and (17), to obtain (see, *e.g.*, refs. [8,12,13])

$$\frac{\partial h}{\partial t} + \frac{\partial}{\partial x}\int_0^{h(x,t)} v_x\,\mathrm{d}z = 0. \tag{20}$$

This condition constitutes a more convenient form of the kinematic condition (17) and assures the conservation of mass on a domain with a deflecting upper boundary. Replacing the relation (19) into (20), one gets the film equation

$$\frac{\partial h}{\partial t} = -\frac{\partial}{\partial x}\left[\frac{2}{3}hv_S - \frac{1}{6}\Gamma' h^2\right]. \tag{21}$$

The evolution equation for v_S is given by the Navier-Stokes equation (13) written at the upper boundary $z = h(x,t)$

$$-\frac{\partial p}{\partial x} + \frac{2\Gamma'}{h} - \frac{2v_S}{h^2} = 0. \tag{22}$$

For describing Marangoni flows between two approaching liquid films of different materials, one introduces the molar fraction c of one of the components of the two miscible fluids. As usual, the surface tension σ is taken as linear function of the bulk concentration $c(x,t)$ [35,36]

$$\sigma = \sigma_0 - \sigma_C c, \tag{23}$$

with σ_0 the inverse capillary number and $\sigma_C = -\frac{\mathrm{d}\sigma}{\mathrm{d}c}$ the Marangoni number. To close the system, the diffusion equation for the concentration field c is taken into account

$$\frac{\partial c}{\partial t} + \bar{v_x}\frac{\partial c}{\partial x} = \tilde{D}\frac{\partial^2 c}{\partial x^2}\,, \tag{24}$$

where $\bar{v_x} = \frac{2}{3}v_S - \frac{1}{6}\Gamma' h$ represents the horizontal velocity averaged in the z-direction and $\tilde{D} = O(\delta^2)$ can be neglected.

2.2 Results and discussions

Equations (21), (22) and (24) are solved numerically in two dimensions using a finite-difference method with 500 mesh points in the x-direction [37,38] for the following

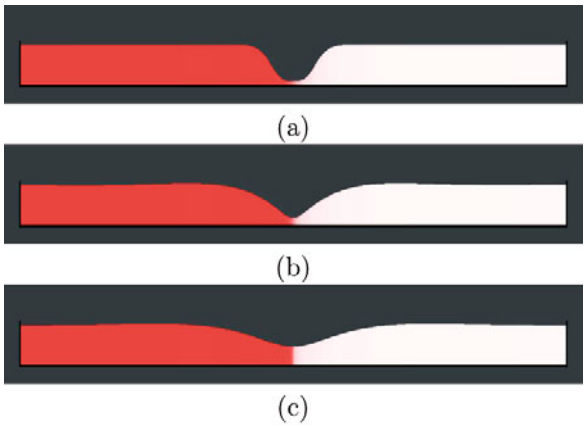

Fig. 5. (Color online) Time series for the fusion of two thin liquid layers without Marangoni effect at the upper surface: (a) $t = 0$; (b) $t = 0.43\,\mathrm{s}$; (c) $t = 0.8\,\mathrm{s}$. The computer simulations result from the lubrication approximation with $h(t = 0) = 0.2\,\mathrm{mm}$, $l = 2\,\mathrm{mm}$, $\rho = 10^3\,\mathrm{kg/m^3}$, $\nu = 5 \cdot 10^{-6}\,\mathrm{m^2/s}$, and $\sigma = 0.05\,\mathrm{N/m}$.

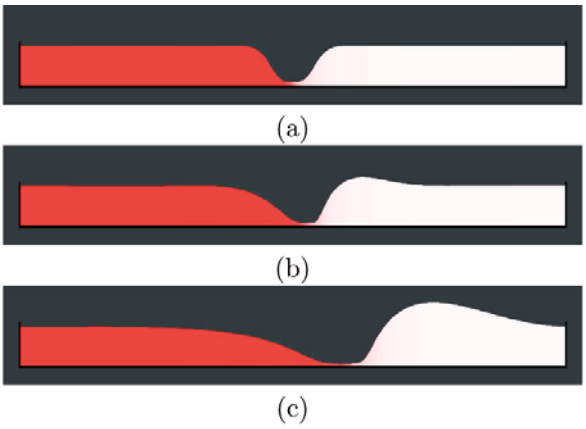

Fig. 6. (Color online) Coalescence of two thin liquid films consisting of perfectly miscible liquids with different surface tensions. At $t = 0$ liquid 1 (left-hand side) has the surface tension coefficient $\sigma_1 = 0.045\,\mathrm{N/m}$ and liquid 2 (right-hand side) has $\sigma_2 = 0.05\,\mathrm{N/m}$. A surface flow caused by Marangoni forces pushes the bridging film at the right and delays the layers fusion: (a) $t = 0$; (b) $t = 0.17\,\mathrm{s}$; (c) $t = 1.1\,\mathrm{s}$. The computer simulations are given by the lubrication theory with $h(t = 0) = 0.2\,\mathrm{mm}$, $l = 2\,\mathrm{mm}$, $\rho = 10^3\,\mathrm{kg/m^3}$, and $\nu = 5 \cdot 10^{-6}\,\mathrm{m^2/s}$.

non-dimensional parameters: the aspect ratio $\delta = 0.1$, the inverse capillary number $\sigma_0 = 400$, and the Marangoni number $\sigma_C = 40$.

That means, for the problem studied in our paper, we have two liquid layers of the same initial height $h(t = 0) = 0.2\,\mathrm{mm}$, the same density $\rho = 10^3\,\mathrm{kg/m^3}$, and the same kinematic viscosity $\nu = 5 \cdot 10^{-6}\,\mathrm{m^2/s}$ connected through a very thin liquid channel $h_i = 20\,\mu\mathrm{m}$ (the contact angle is $\theta = 0°$). The lateral length of the system is $l = 2\,\mathrm{mm}$.

In the lateral direction symmetric boundary conditions are taken for all variables. At the initial moment $t = 0$ the molar fraction is homogeneous in each layer with $c_1 = 1$ for liquid 1 (on the left side in figs. 5 and 6) and $c_2 = 0$ for liquid 2 (on the right side in figs. 5 and 6). Two situations are investigated: without and with Marangoni effects at the upper surface.

Figure 5 shows the coalescence without Marangoni flow (with $\sigma_C = 0$ in relation (23), both liquids have the same surface tension $\sigma = 0.05\,\mathrm{N/m}$). In this case the system tends to minimize the free energy by forming in a late state of evolution only a single liquid layer. The bridging film grows up from $h_i = 20\,\mu\mathrm{m}$ to $h = 0.2\,\mathrm{mm}$ without lateral pushing effects inside the layers.

Next we concentrate on the same two-layer geometry with surface tension gradients along the free surface ($\sigma_C = 40$). The Marangoni effect will be induced by the concentration gradient (see relation (23)). Liquid 1 has the surface tension coefficient $\sigma_1 = 0.045\,\mathrm{N/m}$ and liquid 2 has $\sigma_2 = 0.05\,\mathrm{N/m}$ (as in the experiments presented in fig. 2). A Marangoni flow occurs from the liquid with lower surface tension to the liquid with higher surface tension (from the left to the right in the panels depicted in fig. 6) which pushes the bridging channel between the two liquid layers to the right with velocity $v_{\mathrm{bridge}} = 2.9 \cdot 10^{-3}\,\mathrm{m/s}$ (from panel (a) to panel (c)). The maximal velocity in the bridging layer is around $v = 10^{-2}\,\mathrm{m/s}$. The Marangoni flow from one liquid to another, in accord with the mass conservation in the system, causes a delay in the growth of the connecting film and, therefore, in the fusion between the two liquid layers.

The lateral drop profiles displayed in fig. 3 show that the contact angles of both drops are approximately the same before the drop contact. After the initial contact and during the delayed coalescence the drop surface profiles become asymmetric in the interaction region. Between the two interacting drops, the apparent contact angle decreases for the drop with lower surface tension and increases for the drop with higher surface tension. The experimentally observed shape of the drop surfaces in the vicinity of the drop contact is remarkably similar to the shape obtained from the simulation (see figs. 6b, c and also figs. 8c, d from sect. 3).

Comparing the bridge velocities between these simulations and the experiments, we find the same order of magnitude, although the simulated value exceeds the experimental one by a factor of ≈ 2. The dissipation for a moving droplet occurs mostly in the contact line region [39, 40], *i.e.* next to the connecting bridge between the drops and on each opposing side. The motion-retarding effect of the contact lines is missing completely in the simulations, which explains the higher value for the bridge velocity.

3 Phase field theory

3.1 Governing equations

The lubrication theory is valid for small contact angles and small Reynolds numbers in the layers. In the following we plan to develop a scheme for studying the same

phenomenon using the phase field theory. In this approximation there are no restrictions regarding the contact angles or the Reynolds numbers. We will consider similar situations as shown in the previous section for two sessile perfectly miscible liquid droplets in contact on a solid substrate.

In order to see how one can get the two initial liquid droplets sitting on the solid substrate, using the phase field formalism, we study first a liquid in the gas atmosphere. The phase field theory treats the liquid-gas system continuously by taking an order parameter to distinguish between the coexisting phases. The most natural phase field variable is the density ρ, scaled by the liquid density. So $\rho = 1$ designates the liquid phase and $\rho \approx 0$ the gas bulk. The basic equations consist of the Navier-Stokes equations including phase field terms for assuring a consistent shear stress tensor at the liquid-gas interface (see, *e.g.*, refs. [18, 26,41,42])

$$\rho \frac{\mathrm{d}\boldsymbol{v}}{\mathrm{d}t} = -\boldsymbol{\nabla} p + \rho \boldsymbol{\nabla} \left(\boldsymbol{\nabla} \cdot (\mathcal{K} \boldsymbol{\nabla} \rho) \right) + \boldsymbol{\nabla} \cdot \boldsymbol{\tau} \qquad (25)$$

and the continuity equation

$$\frac{\partial \rho}{\partial t} + \boldsymbol{\nabla} \cdot (\rho \boldsymbol{v}) = 0, \qquad (26)$$

with $p = \rho\, \partial f(\rho)/\partial \rho - f(\rho)$ denoting the thermodynamic pressure (f the free-energy density for the homogeneous phases). The second term on the right-hand side denotes the Korteweg stress, first introduced in [43] and later on studied by several authors (see refs. [44–46], and references therein). The Korteweg stress describes the contribution of the capillary forces and represents in the phase field formalism the substitute of the kinematic boundary condition at the liquid-gas interface (eq. (6) from sect. 2). The third term on the right-hand side in eq. (25) introduces the viscous stress tensor for a compressible fluid, with the components

$$\tau_{ij} = \rho \nu \left(\frac{\partial v_i}{\partial x_j} + \frac{\partial v_j}{\partial x_i} - \frac{2}{3} \delta_{ij} \boldsymbol{\nabla} \cdot \boldsymbol{v} \right),$$

where ν represents the kinematic viscosity and δ_{ij} is the Kronecker delta.

To account for the two stable states liquid and gaseous, we chose [42]

$$f(\rho) \sim \rho^2 (\rho - 1)^2 \qquad (27)$$

and the control of the surface tension coefficient will be done through the gradient energy term $\mathcal{K}(\partial\rho/\partial z)^2/2$ ($\mathcal{K}$ is the gradient energy coefficient) [47]

$$\sigma = \int_{-\infty}^{+\infty} \mathcal{K} \left(\frac{\partial \rho}{\partial z} \right)^2 \mathrm{d}z. \qquad (28)$$

We treat drops and bubbles using the phase field formalism. For this geometry one has no analytical solution for the stationary state. Instead, one can solve the problem numerically, starting from an initial noise density

$$\rho(x, z) = a\, \xi(x, z),$$

where a is the noise intensity, and $\xi(x, z)$ is a uniformly random distribution between 0 and 1. A randomly distributed initial density may act as seeds for phase separation in the van der Waals fluid. The small nuclei start to grow and, ultimately, drops or bubbles are found by nucleation and coarsening. The system evolves to drops in a gaseous or bubbles in a liquid, depending on the total mass (for more details, see [29,30]). With an adequate choice of the mass in the system (varying the noise amplitude a) one obtains after a while a stationary liquid droplet in the gas. At late stages of phase separation, after the fluid has developed well-defined liquid/gas domains separated by interfaces, the Korteweg stress from eq. (25) contains the usual Marangoni force, as shown by Jasnow and Vinals [41] and Borcia and Bestehorn [26].

The boundary conditions for the density field at the solid walls play an important role for the contact angle at the solid surface and determine the position of the droplet. In our model we control the contact angle through the density at the solid boundary ρ_S. Pismen and Pomeau [42] assume that, for solid-fluid interactions short ranged compared to the thickness of the diffuse liquid-gas interface, the only condition enforced on the solid surface (placed at $z = 0$) is

$$\rho = \rho_S. \qquad (29)$$

ρ_S describes the fluid-solid interactions. A flat solid surface with variable wettability (and variable thickness of the precursor film) can be realized varying ρ_S in the range $0 < \rho_S < 1$. Large values for ρ_S correspond to small contact angles (and thin precursor films) and vice versa. In [42] an analytical formula is derived which relates the static contact angle θ to the solid density ρ_S

$$\cos\theta = -1 + 6\,\rho_S^2 - 4\,\rho_S^3, \qquad (30)$$

recently numerically verified through phase field simulations [33]. So, with an appropriate choice of the noise amplitude a and ρ_S ($\rho_S > 0.5$), one can simulate a liquid droplet with a given height h sitting on a hydrophilic surface under a given contact angle θ.

Next we consider two liquid droplets of the same density ρ, the same height h and the same contact angle θ, connected through a precursor film. The two sessile droplets are numerical solutions of eqs. (25), (26), achieved as described above. The two drops consist of different, but perfectly miscible materials. For this situation one needs a second-order parameter which distinguishes between the two miscible liquids. The second-order parameter will be the molar fraction c, assumed to be $c = 1$ for droplet 1 in fig. 1 and $c = 0$ for droplet 2.

As soon as the two droplets are in contact, mixing of the two compounds will commence by convection. The Marangoni effect induced by surface tension difference between the two mixing liquids is taken into consideration by the non-classical term in the Navier-Stokes equation (25). As the surface tension σ, the parameter $\mathcal{K}$ is taken as linear function on c [35,36]

$$\mathcal{K} = \mathcal{K}_0 - \mathcal{K}_C c. \qquad (31)$$

To close the system, one needs again an equation for the concentration field c, according to (24). We take the diffusion equation for the partial density ρc

$$\frac{\partial(\rho c)}{\partial t} + \boldsymbol{\nabla} \cdot (\rho c \boldsymbol{v}) = D\Delta(\rho c), \tag{32}$$

where D denotes the diffusion coefficient.

3.2 Results and discussions

Equations (25), (26) and (32) are solved numerically in two dimensions (x, z) using a finite-difference method with 400×200 mesh points [37,38]. A similar computational code was developed earlier for 2D phase field models describing floating liquid droplets with applied temperature gradient [29] or static contact angles [33].

We assume two perfectly miscible liquid droplets of the same initial height $h(t = 0) = 0.1\,\mathrm{mm}$, the same density $\rho = 10^3\,\mathrm{kg/m^3}$, and the same kinematic viscosity $\nu = 5 \cdot 10^{-6}\,\mathrm{m^2/s}$ connected through a precursor film of order $10\,\mu\mathrm{m}$. The two droplets are surrounded by a gas with $\rho_v \approx 1\,\mathrm{kg/m^3}$ and are sitting on a hydrophilic rigid surface (at $z = 0$) with $\rho_S = 0.95$. From (30) there follows a contact angle for both droplets of $\theta = 10^\circ$ (similar to the experiment). The system is confined in a box with no-slip conditions for the velocity field at the wall boundaries ($\boldsymbol{v} = 0$). The diffusion coefficient is $D = 10^{-9}\,\mathrm{m^2/s}$ for both liquids and $D = 0$ for the gas bulk. At the initial moment $t = 0$ the molar fraction is homogeneous in each drop with $c = 1$ for liquid 1 and $c = 0$ for liquid 2. In the gas atmosphere we consider also $c = 0$. According to the relation (31), a difference of surface tension appears between the two droplets if $\mathcal{K}_C \neq 0$. As in the previous approximation, two situations are investigated: without and with Marangoni effects at the droplets surface.

Figure 7 shows the coalescence without Marangoni effect (with $\mathcal{K}_C = 0$ in relation (31), both liquids have the same surface tension $\sigma = 0.05\,\mathrm{N/m}$). In this case a usual coarsening phenomenon occurs. The system tends to join the drops, to lower the total surface and, in this way, to minimize the free energy, forming in a late state of evolution only one single liquid droplet. As in fig. 5, the bridging precursor film rests in the middle and starts to grow up in vertical direction from $10\,\mu\mathrm{m}$ to $14\,\mu\mathrm{m}$.

Next we concentrate on the same two-droplet geometry with surface tension gradients at the free surface. Drop 1 (left side on the panels in fig. 8) has a lower surface tension than drop 2 (right side on the same panels). Liquid 1 has the surface tension coefficient $\sigma_1 = 0.045\,\mathrm{N/m}$ and liquid 2 has $\sigma_2 = 0.05\,\mathrm{N/m}$. Owing to the surface tension difference, a surface flow occurs within the droplets from the left to the right on the frames depicted in fig. 8, pushing both drops to the right. The bridging film is pushed from frame (a) to panel (b) with velocity $v_{\mathrm{bridge}} = 2 \cdot 10^{-3}\,\mathrm{m/s}$. The driven flow keeps drop 1 temporarily separated from drop 2, causing a delay in droplet fusion. This situation is also called "chasing droplets", because the two droplets are moving one behind the other in the same direction (in the direction of the Marangoni flow). The maximal velocity in the bridging channel between the droplets is around $1.7 \cdot 10^{-2}\,\mathrm{m/s}$ and the fusion time is 1.3 s (fig. 8e).

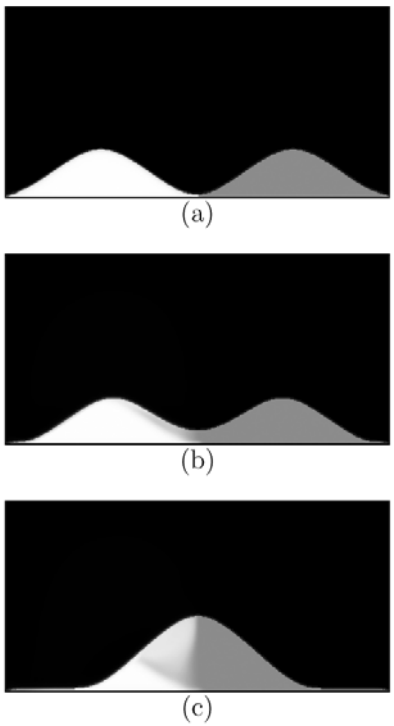

Fig. 7. Coarsening of two drops consisting of different materials without Marangoni effect at the droplets surface. The snapshots correspond to: (a) $t = 0$; (b) $t = 0.8\,\mathrm{s}$; (c) $t = 2\,\mathrm{s}$. The numerical computations are provided by the phase field theory with $h(t = 0) = 0.1\,\mathrm{mm}$, $\rho = 10^3\,\mathrm{kg/m^3}$, $\nu = 5 \cdot 10^{-6}\,\mathrm{m^2/s}$, $\sigma = 0.05\,\mathrm{N/m}$, and $\rho_S = 0.95$, the contact angles for both liquids are $\theta = 10^\circ$.

For the situation illustrated in fig. 8e, the single formed drop in the gas box has a non-uniform concentration distribution at the droplet interface. Therefore, this drop slightly oscillates along of the rigid support inside the box —oscillatory motion driven by the concentration gradients at the droplet surface and by the liquid motions inside the drop. Due to diffusion/convection phenomena, a complete homogeneous distribution is reached inside the droplet and the drop comes to the rest on the solid support (fig. 8f).

Comparing fig. 8a-c to the experimental data from fig. 3(b), the initial stage of "chasing droplets" shows a surprisingly good match between simulation and experiment. The bridging film does not grow significantly, and the bridge moves with a velocity that is closer to the experimental value than the one obtained from lubrication theory. Now the dissipation in the shallow regions of the droplets is reproduced more accurately although the off-center parts of the contact line are still not included. Panel (d) from fig. 8 already shows growth in bridge height which could not be observed in the experiment at the same moment of time ($t = 1\,\mathrm{s}$). The growth however is most likely promoted by the right droplet reaching the border of the

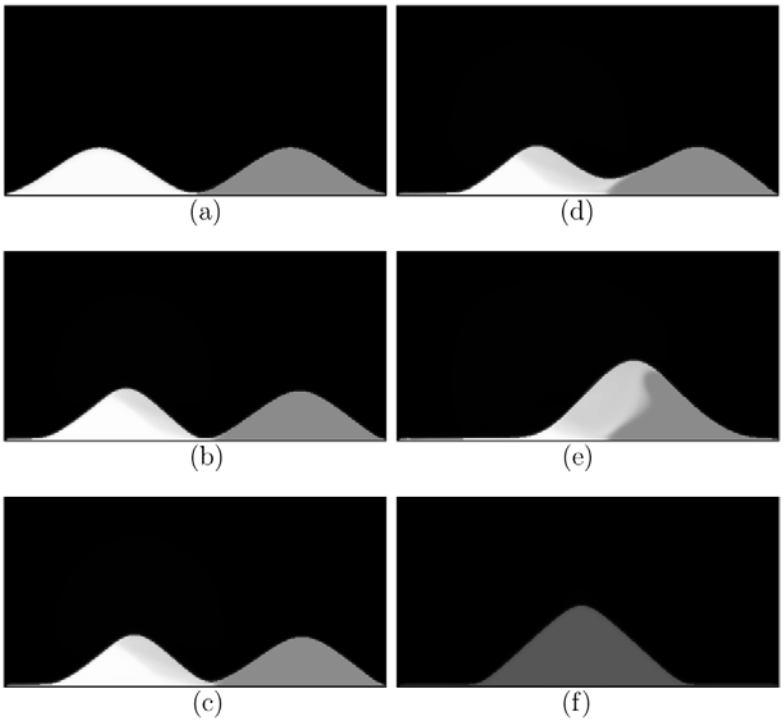

Fig. 8. Phase field simulations on delayed coalescence of two sessile droplets connected through a precursor film with Marangoni effect at the liquid-gas interface. At $t = 0$ drop 1 (left-hand side) has a lower surface tension than drop 2 (right-hand side) ($\sigma_1 = 0.045\,\mathrm{N/m}$, $\sigma_2 = 0.05\,\mathrm{N/m}$): (a) $t = 0$; (b) $t = 0.02\,\mathrm{s}$; (c) $t = 0.8\,\mathrm{s}$; (c) $t = 1\,\mathrm{s}$; (e) $t = 1.3\,\mathrm{s}$; (f) $t = 1000\,\mathrm{s}$ ($h(t = 0) = 0.1\,\mathrm{mm}$, $\rho = 10^3\,\mathrm{kg/m^3}$, $\nu = 5 \cdot 10^{-6}\,\mathrm{m^2/s}$, $\theta = 10°$).

box (fixed boundary conditions), which could also be observed in some experiments where the droplets hit the substrate border.

4 Conclusion

We have proposed two theoretical tools for describing delayed coalescence of two perfectly miscible thin liquid films/drops with low contact angles: a lubrication approximation and a phase field theory. The two methods are completed by quantitative 2D numerical simulations. Computer simulations reproduce well the experimental findings on droplet shape evolution during the delayed coalescence. A direct comparison with the experiment has been done estimating the liquid bridge velocity v_{bridge}, directed towards the thin liquid film/drop with higher surface tension. For both models, the calculated bridging film velocity v_{bridge} is of the same order of magnitude as in experiment.

Both approaches are suitable for describing temporary non-coalescence of droplets. The thin-film model reduces the spatial dimension of the problem by one, the phase field model avoids the interface conditions which are pretty complicated to be imposed for the considered problem. These advantages make the two formulations very attractive in view of the computational simplicity. Both methods have also drawbacks. The phase field approach requires a minimum of points in the diffuse interface in order to modulate a sufficiently sharp interface. Thus, for simulating "big" systems, many mesh points and therefore a longer computation time are necessary. The computing effort in the lubrication approximation is more convenient. However, in the long-wave approach it seems hard to take into account contact angles and contact line associated effects, so that the actual model still cannot estimate the fusion time for the delayed coalescence. This is a weak point of this method which needs further investigation.

Our numerical analysis shows that two liquid drops consisting of the same liquid coalesce fast. If a difference in surface tension occurs between the two drops, sitting on a highly wettable surface, the droplet fusion becomes delayed. The delay is explained by the Marangoni flow established from the droplet with lower surface tension to the droplet with higher surface tension. Computer simulations predict fluid velocities of order cm/s through a very thin channel of $10\,\mu$m bridging two liquid thin films/drops with heights around 0.1 mm. Actually, the delay mechanism reduces to a problem of mass transport across a thin domain connecting two larger reservoirs. The two droplets with a body of different liquids are the reservoirs. The thin liquid channel connecting the reservoirs does not allow a rapid mixing of the two components of the two miscible liquids. So, surface tension gradients (and, therefore, Marangoni flows) are maintained for some time between the droplets. The liquid exchange keeps the drops temporarily separated from each other. The two drops are running one after

the other in the direction of the Marangoni flow ("chasing droplets").

A straightforward task would be to perform simulations of liquid coalescence with different ratios between the surface and viscous forces. Depending on this ratio different kinds of delayed coalescence are expected from "chasing drops" to "droplets repulsion". An extension of the work to three spatial dimensions is desirable and will be done in a forthcoming paper.

R. Borcia and S. Karpitschka kindly acknowledge financial support of Deutsche Forschungsgemeinschaft.

References

1. D.G.A.L. Aarts, H.N.W. Lekkerkerker, H. Guo, G.H. Wegdam, D. Bonn, Phys. Rev. Lett. **95**, 164503 (2005).
2. W.D. Ristenpart, P.M. McCalla, R.V. Roy, H.A. Stone, Phys. Rev. Lett. **97**, 064501 (2006).
3. N. Kapur, P.H. Gaskell, Phys. Rev. E **75**, 056315 (2007).
4. H. Riegler, P. Lazar, Langmuir **24**, 6395 (2008).
5. G.F. Christopher, J. Bergstein, N.B. End, M. Poon, N. Nguyen, S.L. Anna, Lab Chip **9**, 1102 (2009).
6. D.H. Bangham, Z. Saweris, Z. Trans, Faraday Soc. **34**, 554 (1938).
7. S. Karpitschka, H. Riegler, Langmuir **26**, 11823 (2010).
8. A. Oron, S.H. Davis, S.G. Bankoff, Rev. Mod. Phys. **69**, 931 (1997).
9. I.D. Borcia, R. Borcia, M. Bestehorn, Europhys. Lett. **75**, 112 (2006).
10. M. Bestehorn, A. Pototsky, U. Thiele, Eur. Phys. J. B **33**, 457 (2003).
11. A. Pototsky, M. Bestehorn, D. Merkt, U. Thiele, Phys. Rev. E **70**, 025201 (2004).
12. D. Merkt, A. Pototsky, M. Bestehorn, U. Thiele, Phys. Fluids **17**, 064104 (2005).
13. M. Bestehorn, D. Merkt, Phys. Rev. Lett. **97**, 127802 (2006).
14. U. Thiele, E. Knobloch, New J. Phys. **8**, 313 (2006).
15. U. Thiele, E. Knobloch, Phys. Rev. Lett. **97**, 204501 (2006).
16. L.M. Pismen, J. Eggers, Phys. Rev. E **78**, 056304 (2008).
17. R. Mukherjee, D. Bandyopadhyay, A. Sharma, Soft Matter **4**, 2086 (2008).
18. A.J. Bray, Adv. Phys. **43**, 357 (1994).
19. J.S. Langer, in *Directions in Condensated Matter*, edited by G. Grinstein, G. Mazenco (World Scientific, Singapore, 1986) p. 165.
20. D.M. Anderson, G.B. McFadden, A.A. Wheeler, Annu. Rev. Fluid Mech. **30**, 139 (1998).
21. D.M. Anderson, G.B. McFadden, A.A. Wheeler, Physica D **135**, 175 (2000).
22. R.J. Braun, B.T. Murray, J. Cryst. Growth **174**, 41 (1997).
23. X. Tong, C. Beckermann, A. Karma, Q. Li, Phys. Rev. E **63**, 061601 (2001).
24. A. Karma, D.A. Kessler, H. Levine, Phys. Rev. Lett. **87**, 045501 (2001).
25. A.G. Lamorgese, R. Mauri, Phys. Fluids **21**, 044107 (2009).
26. R. Borcia, M. Bestehorn, Phys. Rev. E **67**, 066307 (2003).
27. R. Borcia, D. Merkt, M. Bestehorn, Int. J. Bifurcat. Chaos **14**, 4105 (2004).
28. R. Borcia, M. Bestehorn, Eur. Phys. J. B **44**, 101 (2005).
29. R. Borcia, M. Bestehorn, Phys. Rev. E **75**, 056309 (2007).
30. R. Borcia, M. Bestehorn, Fluid Dyn. Mater. Process. **3**, 287 (2007).
31. P. Seppecher, Int. J. Engng. Sci. **34**, 977 (1996).
32. D. Jacqmin, J. Fluid Mech. **402**, 57 (2000).
33. R. Borcia, I.D. Borcia, M. Bestehorn, Phys. Rev. E **78**, 066307 (2008).
34. R. Borcia, M. Bestehorn, Langmuir **25**, 1919 (2009).
35. P. Colinet, J.C. Legros, M.G. Velarde, *Nonlinear Dynamics of Surface Tension* (Wiley, Berlin, 2001) p. 127.
36. A.A. Nepomnyashchy, M. Velarde, P. Colinet, *Interfacial Phenomena and Convection* (Chapman & Hall/CRC, Boca Raton, Florida, 2002) p. 262.
37. C. Hirsch, *Numerical Computation of Internal and External Flows*, Vol. **1** (Wiley, New York, 1998) p. 201.
38. M. Bestehorn, *Hydrodynamik und Strukturbildung* (Springer-Verlag, Berlin, 2006) p. 347.
39. S. Moulinet, C. Guthmann, C. Rolley, Eur. Phys. J. B **37**, 127 (2004).
40. S. Iliev, N. Pesheva, D. Iliev, Phys. Rev. E **81**, 011607 (2010).
41. D. Jasnow, J. Viñals, Phys. Fluids **8**, 660 (1996).
42. L.M. Pismen, Y. Pomeau, Phys. Rev. E **62**, 2480 (2000).
43. D.J. Korteweg, Arch. Sci. Phys. Nat. **6**, 1 (1901).
44. N. Bessonov, J.A. Pojman, V. Volpert, J. Engn. Math. **49**, 321 (2004).
45. B. Zoltowski, Y. Chekanov, J. Masere, J.A. Pojman, V. Volpert, Langmuir **23**, 5522 (2007).
46. N. Bessonov, J. Pojman, G. Viner, V. Volpert, B. Zoltowski, Math. Model. Nat. Phenom. **3**, 108 (2008).
47. J.W. Cahn, J.E. Hilliard, J. Chem. Phys. **28**, 258 (1958).